A LETTERS JOURNAL EXPLORING THE FRONTIERS OF PHYSICS

OFFPRINT

^{3}He-free triple GEM thermal neutron detector

G. CLAPS, F. MURTAS, A. PIETROPAOLO, G. CELENTANO, A. VANNOZZI, A. SANTONI, L. QUINTIERI and R. A. RIEDEL

EPL, **105** (2014) 22002

epl

A Letters Journal Exploring the Frontiers of Physics

AN INVITATION TO SUBMIT YOUR WORK

www.epljournal.org

The Editorial Board invites you to submit your letters to EPL

EPL is a leading international journal publishing original, high-quality Letters in all areas of physics, ranging from condensed matter topics and interdisciplinary research to astrophysics, geophysics, plasma and fusion sciences, including those with application potential.

The high profile of the journal combined with the excellent scientific quality of the articles continue to ensure EPL is an essential resource for its worldwide audience. EPL offers authors global visibility and a great opportunity to share their work with others across the whole of the physics community.

Run by active scientists, for scientists

EPL is reviewed by scientists for scientists, to serve and support the international scientific community. The Editorial Board is a team of active research scientists with an expert understanding of the needs of both authors and researchers.

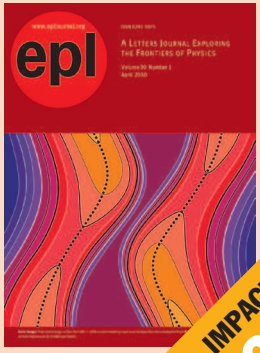

IMPACT FACTOR 2.753*

*As ranked by ISI 2010

IMPACT FACTOR
2.753*
* As listed in the ISI® 2010 Science Citation Index Journal Citation Reports

OVER
500 000
full text downloads in 2010

30 DAYS
average receipt to online publication in 2010

16 961
citations in 2010
37% increase from 2007

"We've had a very positive experience with EPL, and not only on this occasion. The fact that one can identify an appropriate editor, and the editor is an active scientist in the field, makes a huge difference."

Dr. Ivar Martinv
Los Alamos National Laboratory, USA

Six good reasons to publish with EPL

We want to work with you to help gain recognition for your high-quality work through worldwide visibility and high citations.

1. **Quality** – The 40+ Co-Editors, who are experts in their fields, oversee the entire peer-review process, from selection of the referees to making all final acceptance decisions
2. **Impact Factor** – The 2010 Impact Factor is 2.753; your work will be in the right place to be cited by your peers
3. **Speed of processing** – We aim to provide you with a quick and efficient service; the median time from acceptance to online publication is 30 days
4. **High visibility** – All articles are free to read for 30 days from online publication date
5. **International reach** – Over 2,000 institutions have access to EPL, enabling your work to be read by your peers in 100 countries
6. **Open Access** – Articles are offered open access for a one-off author payment

Details on preparing, submitting and tracking the progress of your manuscript from submission to acceptance are available on the EPL submission website **www.epletters.net**.

If you would like further information about our author service or EPL in general, please visit **www.epljournal.org** or e-mail us at **info@epljournal.org**.

EPL is published in partnership with:

European Physical Society | Società Italiana di Fisica | EDP Sciences | IOP Publishing

A Letters Journal Exploring the Frontiers of Physics

January 2014

EPL, **105** (2014) 22002 www.epljournal.org
doi: 10.1209/0295-5075/105/22002

^{3}He-free triple GEM thermal neutron detector

G. Claps[1], F. Murtas[1,2], A. Pietropaolo[3,4(a)], G. Celentano[3], A. Vannozzi[3], A. Santoni[3], L. Quintieri[5] and R. A. Riedel[6]

[1] *Istituto Nazionale di Fisica Nucleare - Laboratori Nazionali di Frascati - Via Enrico Fermi 40, 00044 Frascati (Rome), Italy*
[2] *CERN - CH-1211 Geneva 23, Switzerland*
[3] *ENEA Centro Ricerche Frascati - Via Enrico Fermi 45, 00044 Frascati (Rome), Italy*
[4] *MIFP, Mediterranean Institute of Fundamental Physics - Via Appia Nuova 31, 00040 Marino (Rome), Italy*
[5] *ENEA Centro Ricerche Casaccia - Via Anguillarese 301, 00123 S. Maria di Galeria (Rome), Italy*
[6] *Oak Ridge National Laboratory - 2008 MS-6466, Oak Ridge, TN 37831-6466, USA*

received 13 November 2013; accepted in final form 12 January 2014
published online 10 February 2014

PACS 29.40.-n – Radiation detectors
PACS 29.40.Cs – Gas-filled counters: ionization chambers, proportional, and avalanche counters
PACS 29.30.Hs – Neutron spectroscopy

Abstract – A novel type of thermal neutron detector based on the gas electron multiplier (GEM) technology is presented in the framework of the research and development activity on the ^{3}He replacement for neutron detection. The device relies on a series of boron-coated alumina sheets placed perpendicularly to the incident neutron beam direction. The detector, named side-on GEM (S-GEM), was tested on beam at the High Flux Isotope Reactor at the Oak Ridge National Laboratory (US) to assess its performance in terms of beam position resolution, efficiency and signal-to-background (S/B) ratio as compared to a 10 bar ^{3}He tube for sub-thermal neutrons. Using 3 mm wide PADs, a sub-millimeter position resolution was obtained. The achieved efficiency is about 30% with a quite good S/B ratio. The obtained results demonstrate the effectiveness of the proposed detector configuration to achieve a good spatial resolution and, in the perspective, a higher thermal neutron efficiency, comparable to ^{3}He tubes typically used for diagnostic in nuclear reactors. The main issues to be addressed to reach the goal, mostly related to boron coating procedures and characterization, are also pointed out.

Introduction. – The global shortage of ^{3}He for neutron detection purposes triggered an intense and interesting research and development activity worldwide to find out effective solutions. Different approaches have been proposed so far such as the use of boron or lithium fluoride loaded detectors [1–6]. Although reactions producing charged particle in the final state are widely investigated, also thermal neutron radiative capture has been recently used [5,7,8].

In this paper, a particular gaseous detector, namely the gas electron multiplier (GEM) [9], is described. In particular, a triple GEM device [10,11] was equipped with a sequence of alumina sheets, coated by boron films on both surfaces, acting as neutron–charged-particle converters. The detector window is made on the frames of the GEM foils, so that the neutron beam can impinge laterally (that is, perpendicularly to the wider sheet surface) onto the detector rather than frontally, as typically happens in other applications [12,13]. The device, conceived and assembled at the Istituto Nazionale di Fisica Nucleare (INFN-Laboratori Nazionali di Frascati) and already named as side-on GEM (S-GEM) [14], was tested at the High Flux Isotope Reactor (HFIR) (Oak Ridge National Laboratory, US) [15,16].

Experimental set-up and measurements. – *GEM detector configuration.* As shown in fig. 1, the detector is made of three main elements: the anode, the three GEM foils and the cathode. These are stacked in order to have a properly sealed chamber with only two holes for the gas flowing through it. The internal side of the anode is divided in 4×32 readout pads, with an area of $3 \times 24\,\mathrm{mm}^2$ each.

This device is an upgrade of the first side-on GEM thermal neutron detector, already named S-GEM, described in ref. [14]. The latter was conceived to understand the main

(a) E-mail: antonino.pietropaolo@enea.it

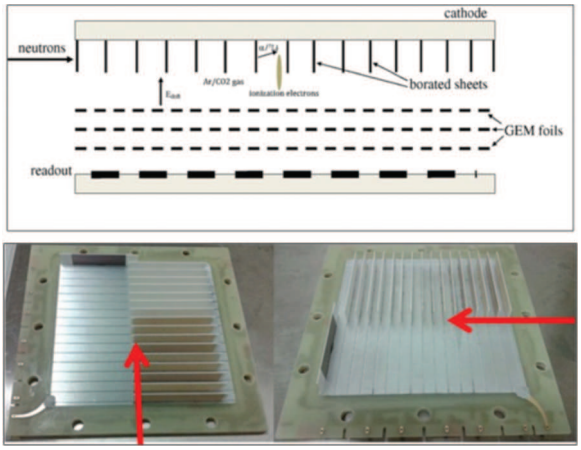

Fig. 1: (Color online) Upper panel: schematic of the S-GEM with borated-sheets arrangement on the aluminum cathode. In typical GEM detector applications the radiation field impinges from the top of the drawing. Lower panel: picture showing the actual sheets configuration before detector assembly. The arrows indicate the direction of the neutron beam.

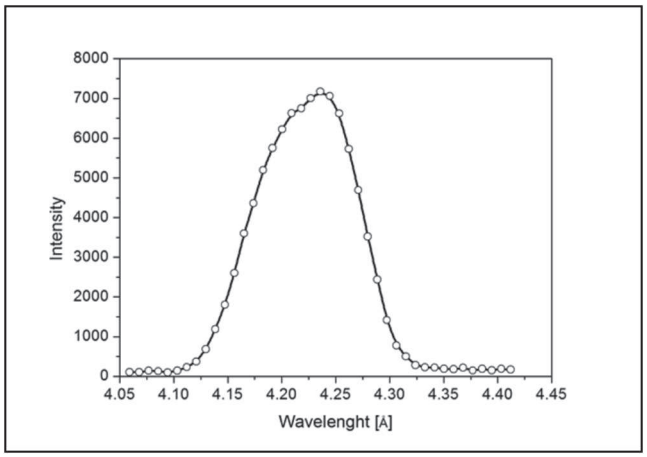

Fig. 2: Neutron spectrum as a function of the neutron wavelength provided by the HFIR reactor along the CG1A extraction line.

features of the device, in terms of linearity and efficiency. In that prototype the arrangement of the readout pads was not well matched with the sheets geometry, achieving a millimeter spatial resolution. In the present device the readout pads arrangement was chosen to achieve a better spatial resolution along the beam direction, this issue being addressed in the presented tests.

Located on the external side, there is the readout electronics consisting of a set of eight CARIOCA chip cards and a FPGA mother board, the details being described in ref. [12]. The cathode is an aluminum plate, that on the internal side facing the gas mounts 16 borated alumina sheets on one half of the active volume of the drift region and one borated alumina sheet on the other half side. Each sheet is 50 mm long, 10 mm high and 400 μm thick while the drift region is 12 mm high, so that the sheets do not touch the fist GEM foil. An epoxy glass window was obtained on the lateral side of the drift region and parallel to the borated sheets. It has an area of $10 \times 1\,\mathrm{cm}^2$ and a thickness of 0.5 mm. This setup allows neutrons to impinge onto the detector laterally and to exploit all the converting surfaces. A detector window is placed on the side of the anode with 32 pads. In this way the detector is able to measure also the position of small-spot beams impinging on the side-on window.

The sheets were coated on both sides using ^{10}B. The coating was obtained by means of electron beam evaporation techniques, carried out in a vacuum chamber equipped with a multi-crucible Thermionics 10 kW electron beam system. The deposition thickness was about 1 μm. This sheets configuration was chosen using as reference the device (the S-GEM prototype) described in ref. [14]. The side with a single sheet allows us to evaluate gamma background and the single-sheet efficiency with respect to the 16-sheets arrangement.

When a neutron is absorbed into the ^{10}B layer, an alpha particle and a ^{7}Li ion are produced following the reactions $n + {}^{10}\mathrm{B} \rightarrow {}^4\mathrm{He} + {}^7\mathrm{Li}$ ($Q = 2.8\,\mathrm{MeV}$, BR = 7%) or $n + {}^{10}\mathrm{B} \rightarrow {}^4\mathrm{He} + {}^7\mathrm{Li} + \gamma$ (478 keV) ($Q = 2.3\,\mathrm{MeV}$, BR = 93%). These charged particles ionize the Ar/CO_2 gas mixture (70%/30%) in the drift region of the detector thus producing secondary electrons. These, moved by the electric field in this region, reach the three GEM foils where they are proportionally multiplied in cascade, inducing a detectable signal in the pad-based readout.

Measurements and data analysis. The detector was characterized at the CG1A beam line at the HFIR facility, a nuclear research reactor located at Oak Ridge National Laboratory (ORNL, Oak Ridge, Tennessee, US). HFIR operates at 85 MW power and is one of the highest-flux reactor-based sources of neutrons for condensed-matter research in the United States. CG1A is a detector test station providing 4.2 Å neutrons at an estimated flux of $2 \times 10^6\,n\,\mathrm{cm}^{-2}$. The neutron beam used for the measurements extended on an irradiation area of $5 \times 5\,\mathrm{cm}^2$ and had an angular divergence lower than one degree, making it extremely useful to characterize resolution, uniformity, distortion and performance with a high neutron flux.

The HFIR neutron spectrum, shown in fig. 2, features a Maxwell-Boltzmann distribution peaked at $\lambda = 4.23$ Å ($E \sim 4.57$ meV) with a Full Width at Half-Maximum (FWHM) of about 0.11 Å.

This spectrum is measured using the time-of-flight analysis. This is accomplished by using a pinhole neutron chopper operating at about 100 Hz and a ^{3}He detector approximately 1.5 m from the chopper. The time-of-flight spectrum is converted to wavelength using a well-known constant.

The main goals of our experimental tests were to evaluate linearity and accuracy in beam positioning and to measure the detector efficiency.

For beam intensity tests, the experimental set-up is sketched in fig. 3(a): a 2 mm thick borated aluminum mask

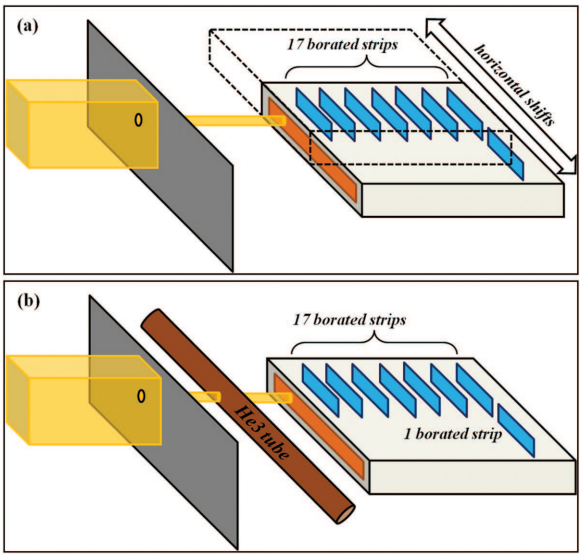

Fig. 3: (Color online) (a) Schematic layout of the experimental set-up used for the beam position scanning of the S-GEM detector. Also shown is the borated aluminum (holed) mask used to produce a pencil beam configuration. (b) Experimental set-up used for efficiency measurements. This time an ^{3}He tube is placed between the mask and the S-GEM detector which is turned off during ^{3}He tube measurements.

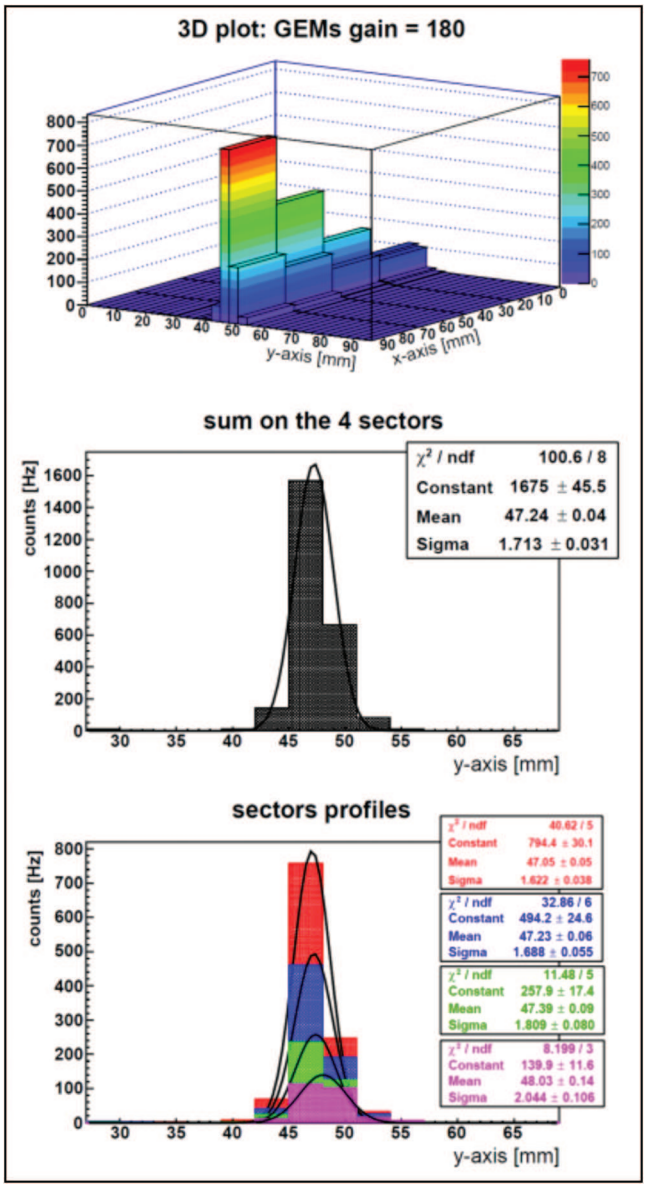

Fig. 4: (Color online) (a) 3D beam profiles measured during the detector position scan along the its active window; (b) a beam profile on the Y-section, obtained summing all the counts on the pads along X-direction; (c) beam profiles obtained on the 32 Y-pads on each of the four pads sectors along the X-direction.

was placed at a distance of about 2 m from the source to provide an almost complete absorption of about 99.7% of the neutrons over the whole spectrum shown in fig. 2. The mask features a 2.5 mm diameter hole to provide a collimated beam for positioning tests described below. Beyond the screen there was the S-GEM detector mounted on a mobile support so that it could be moved along the horizontal direction parallel to the window. During beam positioning tests the detector was moved in steps of 10 mm (with an accuracy of better than 10 μm) scanning in such a way all the window by the small-hole beam. Then to make efficiency measurements, an ^{3}He tube was placed in front of the GEM detector: it is 1 cm in diameter and 30 cm long with 10 bar pressure, providing an efficiency close to 1 at the neutron spectrum peak. During the GEM measurements the ^{3}He detector was moved away, while during the measurements with the ^{3}He tube the GEM detector was not recorded. The GEM measurements were made in two different positions with respect to the beam passing through the mask hole in order to irradiate the 16-sheets region and the single-sheet one. To evaluate the overall background sensitivity of both ^{3}He and GEM detectors, the measurements were done also with the mask hole closed.

The S-GEM was operated with a biasing voltage of 870 V, corresponding to a gain of about 180, that allows an effective lowering of the gamma sensitivity as already shown in other experimental tests [11,14]. The ^{3}He tube used a PDT model 20A preamplifier and was biased at about 1200 V. The TTL output of the PDT preamplifier is input into an ORTEC 974 counter and the count rate is the average value over a 100 s counting time. The efficiency of the ^{3}He tube has been verified using a second ^{3}He tube operating under similar conditions with a different PZT amplifier. Dead time loss is not significant in the ^{3}He detector below 10000 counts s^{-1}.

During the detector position scan, a sequence of 3D beam profiles like those shown in fig. 4(a) was measured. The 2D beam profile (fig. 4(b)) was obtained by summing all the counts on the four pads along the X-axis. A Gaussian function was used to fit these profiles: their

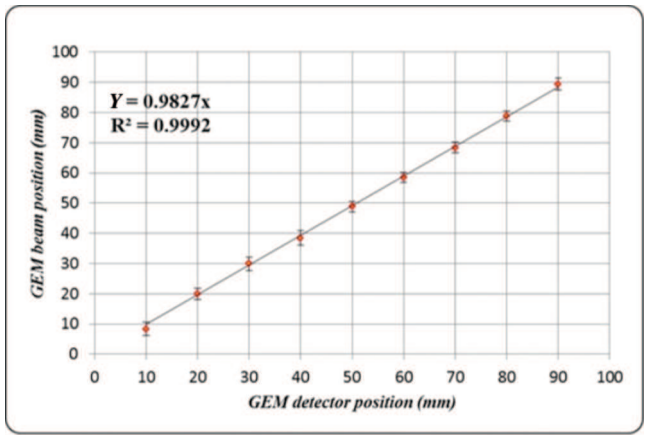

Fig. 5: (Color online) Correlation between detector position and measured beam position value obtained from the Y-axis beam profile.

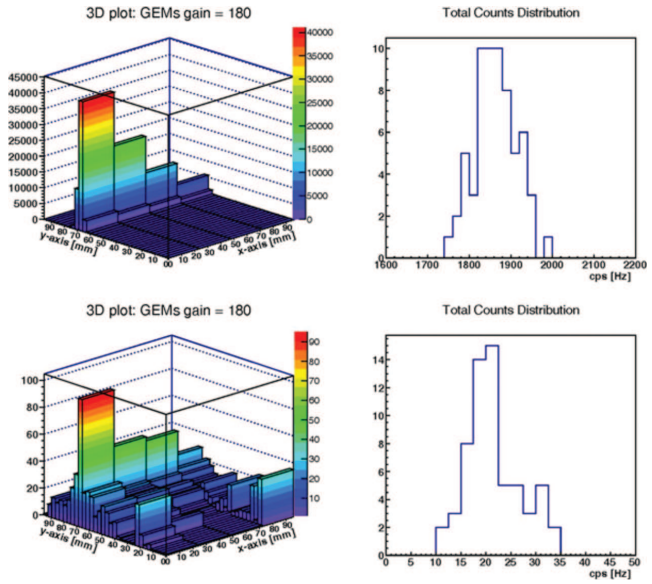

Fig. 6: (Color online) (a) 3D plot of the total counts distribution in the S-GEM in the open pencil beam configuration; (b) histogram of the total counts distribution in the S-GEM obtained summing over the whole set of acquisition triggers of the measurement. Panels (c) and (d) are the same plots of panels (a) and (b) but for the closed pencil beam configuration, *i.e.* background measurements.

central value provides a measure of the beam positions. Figure 4(c) shows the intensity profiles along the X-direction (neutron beam axis) for the four pads rows. The Gaussian fit shows an increase in the FWHM of the beam profile, along the neutron flight path inside the detector, of about 25% between the first and the last pads sector. This is most likely due to a small divergence of the beam. The effect of the scattering of the borated sheets is very small: a theoretical calculation of the scattering power of a borated sheet (the overwhelming contribution is from aluminum), provides a value of 4‰ circa. Neutron scattering off aluminum seems to be not significant in such a way to affect the FWHM of the measured intensity profiles.

Figure 5 shows the correlation between detector position and the measured beam central value. An excellent linear correlation is found, as follows from linear fit with a zero intercept. Considering as negligible the uncertainties in the detector position, it is possible to evaluate the residuals of the measured values with respect to the linear fit. A root mean square of these residuals provides a detector position resolution of about $770 \pm 80\,\mu$m.

The second important issue to be addressed was the evaluation of detector's efficiency on both sides. In what follows we mainly report the results for the 16-sheets and 1-sheet irradiation to be compared to those of the ^{3}He tube.

The S-GEM detector worked using an internal trigger and registered the number of counts over a time window of 1 s after each trigger.

In fig. 6 (upper panel for open hole, and bottom panel for closed hole) the 3D plots represent the cumulative of the counts distribution on each pad obtained summing the counts for each trigger; the plots on the right are the total count distribution recorded by the detector.

Analyzing these distributions, it is possible to calculate the mean of the counts number and its uncertainty for the two beam configurations. Table 1 reports the calculated values of the efficiency and signal-to-background (S/B) ratio for both S-GEM and ^{3}He tube.

Table 1: Signal and background counts for S-GEM and ^{3}He tube detectors and measured values of S/B ratio and efficiency, the efficiency of ^{3}He tube being known by measurements performed previously to the present one.

	S-GEM	^{3}He Tube
Overall mean counts (s^{-1})	1863	6011
Background mean counts (s^{-1})	21	1586
Signal/Background	87.7	2.8
Efficiency (%)	31	99
Single-sheet efficiency (%)	2.8	

The background counts in the S-GEM are mostly due to environmental neutrons (almost an isotropic components and a directional one due to neutron beam, passing through the mask) as the gamma sensitivity at the chosen operation bias is almost null. The higher background sensitivity of the ^{3}He tube, as compared to the S-GEM, is primarily due to the incomplete shielding of 30 cm long tube to background neutrons.

The absolute S-GEM efficiency was calculated as

$$\varepsilon_{\mathrm{GEM}} = \frac{(C_{\mathrm{GEM}} - C_{\mathrm{GEM\text{-}BCKG}})/CS}{(C_{^3\mathrm{He}} - C_{^3\mathrm{He\text{-}BCKG}})/\varepsilon_{^3\mathrm{He}}}, \qquad (1)$$

where C_{GEM} and $C_{\mathrm{GEM\text{-}BCKG}}$ are the overall counts and the background counts in the S-GEM, respectively, while $C_{^3\mathrm{He}}$ and $C_{^3\mathrm{He\text{-}BCKG}}$ are the same quantities for the ^{3}He

tube; $\varepsilon_{^3\mathrm{He}}$ is the ^{3}He tube absolute efficiency (99%) and CS is the cluster size. This last value is a statistical parameter taking into account the possibility for a neutron to fire more than one single pad in the S-GEM detector. Estimation of cluster size has been obtained carrying out measurements with small integration times ($< 20\,\mu$s) and very low intensity beams. These experimental conditions allow to have a single particle for each trigger and make a statistical analysis of number of pads fired. In this case the estimated value at 870 V is about 1.34 ± 0.02.

The evaluated absolute efficiency at 5.1 meV of the S-GEM on the 16-sheets region is 31% $\pm$ 1%, while for the single-sheet region it is found to be (2.8 ± 0.5)%.

The borated sheets were analyzed by X-ray Diffraction (XRD) and X-ray Photoelectron Spectroscopy (XPS) to assess the actual chemical and phase composition of the coating. As can be noted in fig. 1, the boron coatings have different color, from black (for the single-sheet region) to light brown and white (for the 16-sheets region). XRD measurements have revealed the presence of a B_2O_3 component, being larger in white than in darker films.

XPS data were acquired in an Ultra-High Vacuum (UHV) system operating at 4×10^{-8} Pa base pressure. It is equipped with both a non-monochromatic SPECS Mg $K\alpha$ and a VG Al $K\alpha$ monochromatic X-ray source and with a CLAM2 hemispherical analyzer. Two different regions of a borated sheet (labeled as I and II) with a whitish appearance were investigated. In order to probe the film composition at different depths, samples were mildly sputtered in UHV with 1 keV Ar ion energy. The Ar etching rate is estimated to be about 4–5 nm/min. The XPS intensities used for extracting the concentration were obtained by normalizing the area of the background-subtracted core level peaks by the CLAM2 analyzer transmission function [17], by the Scofield cross-section [18] corrected for the angular asymmetry [19] and by the electron mean free path [20]. The relative atomic concentrations (at%), calculated by XPS analysis and summarized in table 2, gave very similar results for the two regions at all the four chosen depths indicating a good uniformity in the film composition. Only 55% of detected atoms is boron, 30% is oxygen and the remaining carbon. The uncertainty for the concentration values is estimated to be $\pm$5%. At a closer examination, in the B1s XPS peak (not shown) it is possible to reveal the presence of two components. The binding energy values of the two features and the chemical shift indicate the presence of metallic B and B_2O_3 with a proportion of about a 60% and 40%, respectively. As far as the single darker sheet shown in fig. 1, a preliminary investigation indicated a concentration of about 80% of boron. More detailed information will be provided on deposition characterization I a forthcoming experimental paper [21].

The borated sheets were obtained in three deposition runs using different sets of boron tablets as evaporation sources. One set was used for the deposition of the films with whitish appearance, whereas a second set of tablets for the black sheet. When mixed tablets were used as source, light-brown films resulted. It is likely that the different fraction of oxide component derives from the tablets. Consider that the sets of tablets were sinterized following two different procedures, so different contents of B_2O_3 can be reasonably expected (the same ^{10}B powder was employed). A more detailed quantitative study to assess the actual chemical composition of tablets is ongoing [21].

Table 2: Relative atomic concentrations extracted by XPS analysis for samples I and II obtained from the same B-coated alumina strip.

Sample	Etching time (min)	Source	B1s (at%)	O1s (at%)	C1s (at%)
I	30	Mg$K\alpha$	51	31	18
I	35	Mg$K\alpha$	51	31	18
I	35	Al$K\alpha$	53	30	16
II	5	Mg$K\alpha$	52	30	18
II	10	Mg$K\alpha$	55	29	16

Conclusions. – The knowledge of the exact chemical composition of the boron coatings is a key point in the evaluation of the device efficiency and its potentiality. The measured efficiency is affected by the presence of a relevant amount of oxygen and carbon contaminations, because the sheets contributed to the neutron–charged-particle conversion process less than expected if pure ^{10}B films were used. This leads to a reduction in the overall device efficiency due to the lowering of the effective ^{10}B content within the deposited films. However, it has to be pointed out that this efficiency reduction mechanism is a technological issue and cannot be ascribed to the device concept.

In order to have a rough evaluation of the effective ^{10}B thickness deposited on the 16 sheets, Monte Carlo simulations of the detector have been performed by Fluka code [14], for different ^{10}B thickness values. The results of these simulations lead to the conclusion that the measured total efficiency corresponds to the one expected for a deposited ^{10}B layer thickness lower than 400 nm on each side of the sheets (with the most probable value around 350 nm). Nevertheless, more accurate simulations are in progress in order to assess more accurately these results.

In order to understand the role of both the deposition material and the shadowing effect (the latter only investigated by means of Monte Carlo simulations) on the efficiency, the strategy should be to change one parameter at once, in the present configuration. Indeed, a new detector will be produced with the same number of sheets, with constant thickness (1 μm) but with a deposition material obtained in a controlled environment so to obtain as much as pure ^{10}B tablets.

In conclusion, we have reported about a S-GEM–based thermal neutron detector tests performed at the HFIR reactor to assess efficiency and spatial resolution of the device. Measurements performed with collimated beams clearly show that the pads arrangement provides a measure of the beam position with sub-millimeter accuracy.

The measured efficiency is about 30% but with a strong indication that a more accurate production of the tablets to avoid (mostly) oxygen contamination of the coating and a mitigation of the shadowing effects (see ref. [14]) by a variable boron thickness along the neutron path inside the detector, should be effective in reaching efficiencies higher than 70% in the present detector configuration.

* * *

The authors warmly acknowledge A. Balla, G. Corradi and D. Tagnani from the electronic group of Istituto Nazionale di Fisica Nucleare (Laboratori Nazionali di Frascati), F. Loprete for the mechanical machining of the cathodes. Mr V. Orsetti (ENEA CR Frascati) is thanked for technical support in XPS measurements. The financial support from the MEPA project is also acknowledged.

REFERENCES

[1] Kouzes R. T., Ely J. H., Lintereur A. T., Siciliano E. R. and Woodring M. L., PNNL Report, No. 19050 (2009).
[2] Lintereur A., Conlin K., Ely J., Erikson L., Kouzes R., Siciliano E., Stromswold D. and Woodring M., *Nucl. Instrum. Methods A*, **652** (2011) 347.
[3] Klein M. and Schmidt C. J., *Nucl. Instrum. Methods A*, **628** (2011) 9.
[4] Tremsin A. S., Feller W. B. and Downing R. G., *Nucl. Instrum. Methods A*, **539** (2005) 278.
[5] Festa G., Pietropaolo A., Grazzi F., Barzagli E., Scherillo A. and Schooneveld E. M., *Nucl. Instrum. Methods A*, **654** (2011) 373.
[6] Barbagallo M., Cosentino L., Greco G., Guardo G., Montereali R. M., Pappalardo A., Scirè C., Scirè S., Vincenti M. A. and Finocchiaro P., *Nucl. Instrum. Methods A*, **652** (2011) 355.
[7] Festa G., Pietropaolo A., Reali E., Grazzi F. and Schooneveld E. M., *Meas. Sci. Technol.*, **21** (2010) 035901.
[8] Pietropaolo A. *et al.*, in prepration.
[9] Saul F., *Nucl. Instrum. Methods A*, **386** (1997) 531.
[10] Murtas F., Buonomo B., Corradi G., Mazzitelli G., Pistilli M., Poli Lener M., Tagnani D. and Valentee P., *Nucl. Instrum. Methods A*, **617** (2010) 237.
[11] Murtas F., Croci G., Pietropaolo A., Claps G., Frost C. D., Perelli Cippo E., Raspino D., Rebai M., Rhodes N. J., Schooneveld E. M., Tardocchi M. and GoriniG., *JINST*, **7** (2012) P07021.
[12] Bonivento W., Jarron P., Moraes D., Riegel W. and Dos Santos F., *Nucl. Instrum. Methods A*, **491** (2002) 233.
[13] Guedes G. P., Breskin A., Chechik R., Vartsky D., Bar D., Barbosa A. F. and Marinho P. R. B., *Nucl. Instrum. Methods A*, **513** (2003) 473.
[14] Pietropaolo A., Murtas F., Claps G., Quintieri L., Raspino D., Celentano G., Vannozzi A. and Frasciello O., *Nucl. Instrum. Methods A*, **729** (2013) 117.
[15] HFIR website: `http://neutrons.ornl.gov/facilities/HFIR/`.
[16] Berry K. D., Bailey K. M., Beal J., Diawara Y., Funk L., Hicks J. S., Jones A. B., Littrell K. C., Pingali S. V., Summers P. R., Urban V. S., Vandergriff D. H., Johnson N. H. and Bradley B. J., *Nucl. Instrum. Methods A*, **693** (2012) 179.
[17] Roosendaal S., *Passivation mechanisms in the initial oxidation of iron by oxygen and water vapor*, PhD Thesis, Utrecht University, The Netherlands, 1999, ISBN 90-393-2250-3.
[18] Scofield J. H., *J. Electron. Spectrosc. Relat. Phenom.*, **8** (1976) 129.
[19] Reilman R. F., Msezane A. and Manson S. T., *J. Electron. Spectrosc. Relat. Phenom.*, **8** (1976) 389.
[20] Seah M. P. and Dench W. A., *Surf. Interface Anal.*, **1** (1979) 2.
[21] Celentano G. *et al.*, in preparation.